Title
Assessing intracranial vascular compliance using dynamic arterial spin labeling

Journal
NeuroImage, 124(Pt A)

ISSN
1053-8119

Authors
Yan, Lirong
Liu, Collin Y
Smith, Robert X
et al.

Publication Date
2016

DOI
10.1016/j.neuroimage.2015.09.008

Peer reviewed

NeuroImage 124 (2016) 433–441

Contents lists available at ScienceDirect

NeuroImage

journal homepage: www.elsevier.com/locate/ynimg

Assessing intracranial vascular compliance using dynamic arterial spin labeling

Lirong Yan [a,*], Collin Y. Liu [b], Robert X. Smith [a], Mayank Jog [a], Michael Langham [c], Kate Krasileva [a], Yufen Chen [d], John M. Ringman [b,e], Danny J.J. Wang [a]

[a] Laboratory of FMRI Technology (LOFT), Department of Neurology, University of California Los Angeles, Los Angeles, CA 90095, USA
[b] Department of Neurology, University of Southern California, Los Angeles, CA, USA
[c] Department of Radiology, University of Pennsylvania, Philadelphia, PA 19104, USA
[d] Department of Radiology, Northwestern University, United States
[e] Mary S. Easton Center for Alzheimer's Disease Research, University of California Los Angeles, Los Angeles, CA 90095, USA

ARTICLE INFO

Article history:
Received 4 February 2015
Accepted 4 September 2015
Available online 10 September 2015

Keywords:
Intracranial vascular compliance
Dynamic arterial spin labeling
Pulse wave velocity
Aging
Cerebral perfusion
Cardiovascular diseases

ABSTRACT

Vascular compliance (VC) is an important marker for a number of cardiovascular diseases and dementia, which is typically assessed in the central and peripheral arteries indirectly by quantifying pulse wave velocity (PWV), and/or pulse pressure waveform. To date, very few methods are available for the quantification of intracranial VC. In the present study, a novel MRI technique for in-vivo assessment of intracranial VC was introduced, where dynamic arterial spin labeling (ASL) scans were synchronized with the systolic and diastolic phases of the cardiac cycle. VC is defined as the ratio of change in arterial cerebral blood volume (ΔCBV) and change in arterial pressure (ΔBP). Intracranial VC was assessed in different vascular components using the proposed dynamic ASL method. Our results show that VC mainly occurs in large arteries, and gradually decreases in small arteries and arterioles. The comparison of intracranial VC between young and elderly subjects shows that aging is accompanied by a reduction of intracranial VC, in good agreement with the literature. Furthermore, a positive association between intracranial VC and cerebral perfusion measured using pseudo-continuous ASL with 3D GRASE MRI was observed independent of aging effects, suggesting loss of VC is associated with a decline in perfusion. Finally, a significant positive correlation between intracranial and central (aortic arch) VC was observed using an ungated phase-contrast 1D projection PWV technique. The proposed dynamic ASL method offers a promising approach for assessing intracranial VC in a range of cardiovascular diseases and dementia.

Introduction

Vascular compliance (VC) represents the ability of a vessel to distend or increase volume in response to an increase in blood pressure (Kelly and Chowienczyk, 2002). This buffering mechanism plays an essential role in the protection of the vascular bed by converting the pulsatile flow in arteries to continuous flow into the capillaries. Aging is accompanied by loss of elastin and increased collagen deposition in vessel walls, which result in the loss of aortic compliance (Lee and Oh, 2010; Mohiaddin et al., 1993; Van Bortel and Spek, 1998). Pathologic changes in the blood vessels can also lead to loss of vascular compliance. The reduction of VC has been regarded as a potentially important marker of a number of diseases with high social and economic impact, such as cardio- and cerebrovascular diseases, hypertension, diabetes, and Alzheimer's disease (AD). For instance, studies have reported that both central VC and peripheral VC provide a sensitive marker for essential hypertension (Laurent et al., 2003; McVeigh et al., 1991). A positive association between arterial stiffness and atherosclerosis was found at various sites along the vascular tree (van Popele et al., 2001). It was also reported that the reduction of VC of both large and small arteries occurs at an early time point in patients with diabetes (Romney and Lewanczuk, 2001). Studies have shown that decrease in aortic VC is an independent predictor of cardiovascular events and Alzheimer's disease (Blacher et al., 1999; Laurent et al., 2001; Meaume et al., 2001a; Sutton-Tyrrell et al., 2005). Therefore, the assessment of VC is useful for a number of clinical indications.

In clinical practice, vascular compliance can be indirectly estimated by the measurement of brachial pulse pressure (i.e. systolic–diastolic blood pressure) (Mackenzie et al., 2002). Applanation tonometry (Nelson et al., 2010; Wilkinson et al., 1998) is a noninvasive and accurate representation of the aortic pressure waveform, which can be

* Corresponding author at: Ahmanson-Lovelace Brain Mapping Center, Department of Neurology, University of California Los Angeles, 660 Charles E Young Dr South, Los Angeles, CA 90095, USA.
E-mail address: lryan737@gmail.com (L. Yan).

http://dx.doi.org/10.1016/j.neuroimage.2015.09.008
1053-8119/

used to estimate arterial stiffness with the measurement of central pressures and augmentation index. Pulse wave velocity (PWV) has emerged as another commonly used method to assess VC, which can be measured by Doppler ultrasound (Sutton-Tyrrell et al., 2005) and MRI (Boese et al., 2000; Laffon et al., 2005; Langham et al., 2011a; Mohiaddin et al., 1993; Wentland et al., 2014). The flow pulse waveforms at two artery sites (such as carotid and femoral arteries) are measured. PWV is then calculated by dividing the path length of the pressure wave between the two sites of arteries by the propagation time of the pulse wave. PWV is considered the best surrogate marker of arterial stiffness which is inversely related to VC. However, PWV quantification is limited to large arterial segments such as the carotid arteries, aortic arch or iliofemoral arteries (Boese et al., 2000; Langham et al., 2011a,b; Mohiaddin, 1992; Mohiaddin et al., 1993; Sutton-Tyrrell et al., 2005; Tanaka et al., 2009).

Mounting evidence suggests that intracranial vascular pathology may be associated with the pathogenesis and progression of cerebrovascular disorders and neurodegenerative diseases. Particularly, in Alzheimer's disease, it has been hypothesized that cerebrovascular dysfunctions may precede and cause amyloid accumulation in the vessel walls as well as impaired clearance of amyloid-β peptide 42 across the blood–brain barrier (BBB) (Hughes et al., 2013; Zlokovic, 2011). Therefore, intracranial VC may offer an important marker for vascular pathology of earliest stages of cerebrovascular diseases and AD. To date, however, very few options exist for non-invasive estimation of intracranial VC. Transcranial Doppler ultrasound (TCD) has been applied for assessing cerebral VC through measuring pulsatile blood flow velocities in large cerebral arteries (e.g., middle cerebral artery (MCA)) (Zhang et al., 2009). However, TCD is operator dependent, and has limited capability for assessing changes in arterial geometry and cerebral blood volume. Furthermore, the MCA may not be accessible to TCD in a considerable fraction of the population.

Arterial spin labeling (ASL) is a noninvasive MRI technique for quantitative measurement of cerebral blood flow (CBF) by magnetically labeling the upstream arterial blood water as an endogenous tracer (Detre et al., 2009; Golay et al., 2004). Recently, a novel non-invasive MRI technique for in-vivo estimation of arterial cerebral blood volume (CBV) has been introduced using dynamic ASL by combining ASL with a cine segmented multi-phase balanced steady-state free precession (bSSFP) sequence (Yan et al., 2012). According to the definition of compliance, VC can be calculated by the change of blood volume due to a given change of blood pressure. In the present study, we propose a novel technique for in vivo assessment of intracranial VC, where dynamic ASL scans were synchronized with the systolic and diastolic phases of the cardiac cycle respectively, and VC can be estimated by changes in arterial CBV (ΔBV) in response to changes in arterial pressure (ΔBP). We evaluated the feasibility of this dynamic ASL technique for assessing intracranial VC in two vascular components of large arteries, small arteries and arterioles. The aging effect on VC and the relationships between intracranial VC with cerebral perfusion as well as aortic PWV were subsequently explored as an initial validation of the proposed technique.

Methods

Assessment of intracranial vascular compliance

A dynamic ASL technique has been developed recently for in-vivo estimation of intracranial arterial CBV, by combining ASL with a cine multi-phase bSSFP sequence which was originally developed for cine cardiac imaging. Technical details of this dynamic ASL technique can be found in Yan et al. (2012). This sequence takes advantage of the phenomenon that the longitudinal magnetization of flowing blood is not or only marginally disturbed by the bSSFP pulse train, given the high contrast of blood signal and inherent flow compensation of the bSSFP sequence (Wu et al., 2010; Yan et al., 2012). Once the blood exchanges into tissue, it becomes quickly saturated by the bSSFP readout as the T2/T1 ratio is much lower in the tissue than in the arterial blood at 3 T. Therefore, the labeled blood behaves like an intravascular contrast agent in the dynamic ASL scan, and arterial CBV can be quantified using the standard tracer kinetic model (Ostergaard et al., 1996) similar to dynamic susceptibility contrast MRI.

Fig. 1 shows the diagram of the proposed dynamic ASL technique. By synchronizing ASL with the peak systolic and early diastolic phases of the cardiac cycle, this technique can measure the arterial CBV at systole and diastole, respectively. VC can be subsequently calculated as the ratio of the change of CBV between systole and diastole and the change in arterial pressure, which was approximated by brachial pulse pressure. Since dynamic ASL is able to estimate arterial CBV in both large and small arteries and even in arterioles, this technique can provide in vivo estimation of both global and regional intracranial VC in different components of the cerebrovascular bed.

MRI experiments

All experiments were carried out on a Siemens Tim Trio 3 T scanner using the product 12-channel head coil. A total of 48 subjects (48.6 ± 18.9 years, 21 males) were recruited in this study, and 12 were excluded due to head motion (see below), resulting in a total of 36 subjects (48.6 ± 20 years, 15 males) that were included in data analyses. All subjects provided written informed consents before they participated in the study. Following standard scout and anatomical MRI, an ECG-triggered time-resolved phase contrast (PC) MRI was performed to measure the blood flow velocity in the internal carotid arteries (ICA), as shown in Fig. 1, with the following parameters: FOV = 220 × 220 mm^2, matrix = 192 × 192, FA = 15°, TE = 5.23 ms, VENC = 100 cm/s, 23 phases with an interval of 50 ms, a single axial slice of 5-mm thickness at the level of C1/C2 was imaged with a scan time of 2 min. A typical profile of mean flow velocity in ICA across a cardiac cycle is shown in Fig. 1. The time delays at peak systole and early diastole were identified in each individual subject (on average 150 ms and 400 ms following the trigger, respectively). Two separate ECG-triggered multi-phase bSSFP ASL scans (Control at systole-Tag at systole; Control at diastole-Tag at diastole) were performed with pulsed spin labeling synchronized with the peak systolic and early diastolic phases by an ECG trigger, respectively. The flow-sensitive alternating inversion recovery (FAIR) scheme was implemented for spin labeling, which was immediately followed by a cine bSSFP readout train. The imaging parameters were: FOV = 220 × 220 mm^2, matrix = 96 × 96, FA = 40°, TE/TR = 1.87/3.74 ms, partial Fourier in the phase encoding direction = 6/8, centric ordering k-space acquisition with 20 lines per segment, and 29 phases from 150 to 2250 ms with an interval of 75 ms. The interval between inversion pulses was approximately 3 s covering 3 to 4 heartbeats. An oblique axial slice of 5-mm thickness (Parallel to AC–PC) at the level of internal capsule was imaged. In each cine bSSFP ASL scan, 8 pairs of label/control acquisitions were collected which took approximately 3 min. The two bSSFP ASL scans at systole and diastole took approximately 6 min. To minimize the head motion during scan, paddings were placed around the head. Before and after the MRI scans, brachial blood pressure (BP) was recorded using a MR compatible cuff sphygmomanometer. ECG leads were placed on subjects' chest to trigger VC scans which were performed in the following 4 experiments.

Exp. 1: assessment of VC in different vascular components

Nine young healthy subjects (21.8 ± 2.6 years, 6 males) were included in Exp. 1. Based on the Bloch equation simulation and experimental data, cine bSSFP based dynamic ASL scans can only measure CBV in arteries and arterioles. Therefore, two ECG-triggered bSSFP ASL scans were performed to assess VC in arteries and arterioles. For comparison, two ECG-triggered Look-locker (LL) echo-planar imaging (EPI) ASL

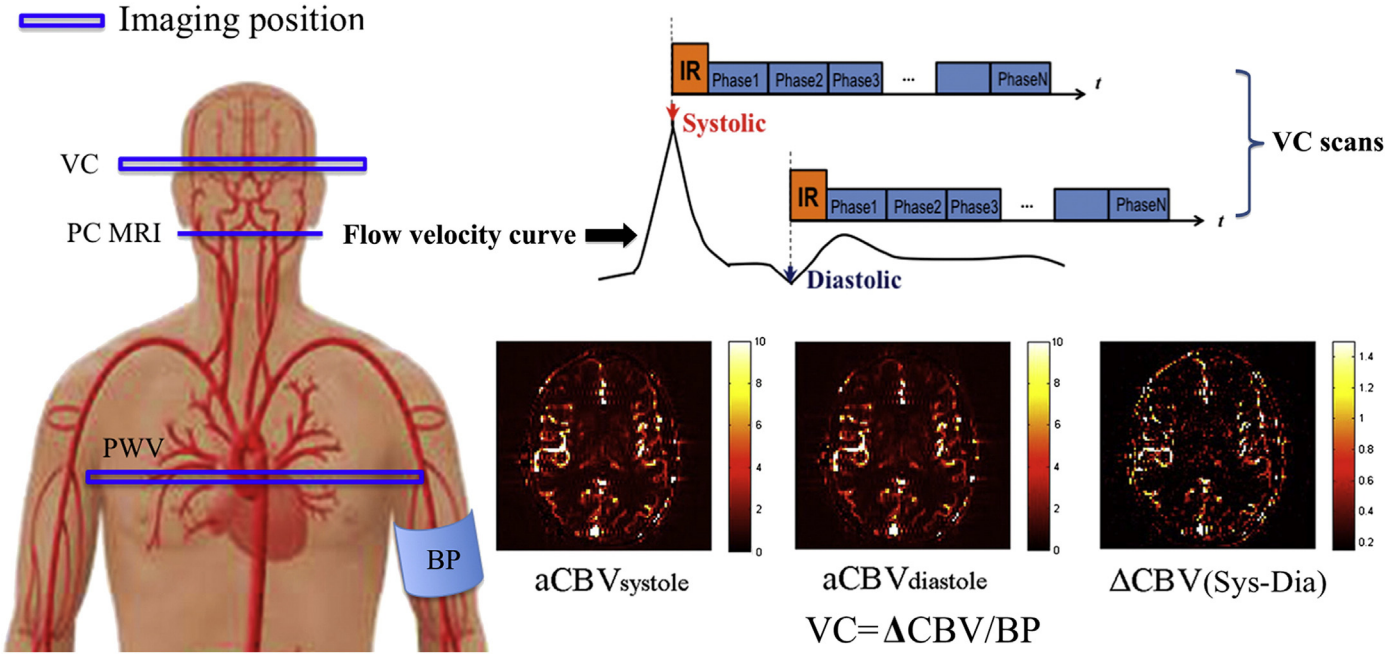

Fig. 1. Illustration of the VC technique applied in the present study. Mean flow velocity curve in the internal carotid artery (ICA) across the cardiac cycle was acquired using PC MRI, by which the delay time at the peak systolic and early diastolic phases was identified. Intracranial VC was assessed by synchronizing dynamic ASL scans with the systolic and diastolic phases of the cardiac cycle using mutil-phase bSSFP scan. Arterial CBV maps at systole and diastole were calculated based on the tracer kinetic model. Intracranial VC was calculated by the changes in arterial CBV between systole and diastole in response to changes in arterial pressure.

scans with flow spoiling gradients (V_{enc} = 8 mm/s, b = 9.3 s/mm^2) were performed to assess dynamic perfusion signal in capillary/tissue, at the same imaging slice position (Chen et al., 2012). For both bSSFP and LL-EPI based ASL scans, spin tagging was applied at peak systole and early diastole respectively. Since vascular signal was suppressed by the flow spoiling gradients, only dynamic perfusion signals in capillaries/tissue were measured using LL-EPI ASL. Imaging parameters for LL-EPI ASL scans were: a single 5 mm slice, FOV = 220 × 220 mm^2, matrix size = 64 × 64, FA = 25°, TE = 35 ms, TI = 330 to 3330 ms with an interval of 300 ms, and 40 pairs of control and label acquisitions with a scan time of approximately 5 min for each LL-EPI scan.

Exp. 2: aging effect on intracranial VC

In Exp. 2, aging effects on VC were investigated by comparison of VC between two groups of young and elderly subjects. Nine elderly subjects without significant systemic, neurologic or psychiatric disorders were included in this experiment (67.8 ± 6.8 years, 3 males). The identical VC and LL-EPI MRI scans of Exp. 1 were performed.

Exp. 3: relationship between intracranial VC vs. cerebral perfusion

This experiment was based on the hypothesis that arterial stiffening will lead to hypoperfusion (Tarumi et al., 2011). Eighteen subjects (52.5 ± 14.4 years, 6 males) were included in Exp 3. Following the two ECG-triggered dynamic bSSFP ASL scans, a 5 min resting-state perfusion MRI scan using pseudo-continuous ASL (pCASL) with background suppressed 3D GRASE readout was performed (Kilroy et al., 2014). Twenty-six 5 mm axial slices were acquired to cover the whole brain with the following imaging parameters: FOV = 220 mm, matrix size = 64 × 64, TE = 22 ms, and TR = 3.5 s. The tagging plane was positioned 90 mm inferior to the center of the imaging slab with a labeling duration of 1500 ms and post-labeling delay of 1500 ms. Thirty pairs of label and control acquisitions were performed with a total scan time of 3 min 30 s.

Exp. 4: relationship between intracranial VC vs. aortic VC

The non-triggered PC-MRI technique with 1D projection was performed for aortic PWV measurement (Langham et al., 2011a,b). The product flex coil was placed on the subjects' chest for PWV scans. As shown in Fig. 2, an axial image across the aortic arch with suitable readout direction was selected to avoid overlapping of ascending and descending aorta as well as pulmonary trunk along the projection. Velocity encoded projections were collected at the ascending and descending aortic segments simultaneously without ECG gating. Imaging parameters were: a single 5 mm axial slice, FOV = 448 × 448 mm^2, readout resolution = 256, TE = 1.66 ms, TR = 3.7 ms, bandwidth = 893 Hz/pixel, flip angle = 15°, VENC = 300 cm/s, and 512 pairs of velocity-encoded projection with a scan time of 4.6 s. Nine subjects (63.6 ± 6.4 years, 5 males) who participated in Exp. 3 underwent the PWV scans.

Imaging data post-processing

Motion control with image outlier rejection

Since the current dynamic ASL technique employed 2D acquisition of a single slice, motion correction was essential for reliable VC measurements. Both within-scan and inter-scan motion effects were assessed. To preserve the original signal intensity, outlier rejection instead of motion correction was performed on the dynamic ASL data. Within the systolic or diastolic dynamic ASL scan, the perfusion-weighted image series were first generated by pair-wise subtraction of control and label acquisitions at each inversion time (TI), and the time course of perfusion-weighted signals of the entire slice were extracted at each TI for each measurement (total 8 measurements). The mean perfusion weighted signal (S_{mean}) and the standard deviation (SD) were calculated at each TI across measurements. If the time course of

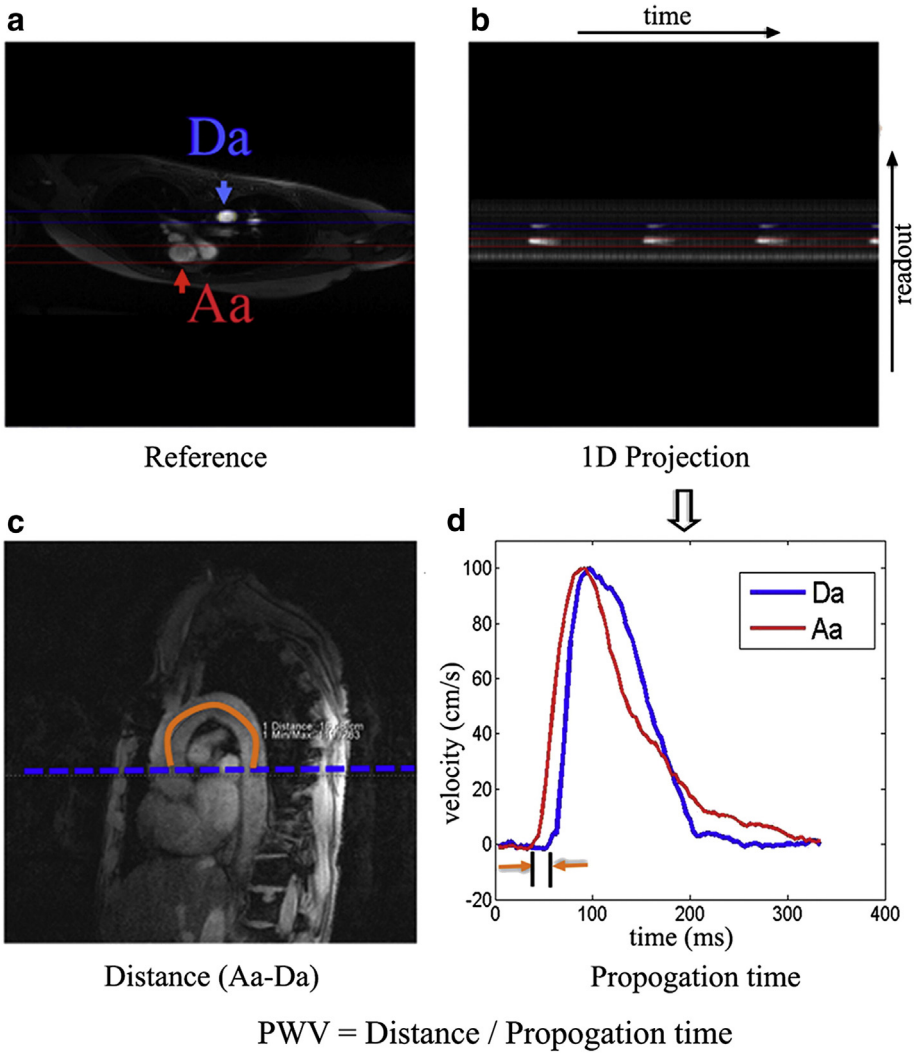

Fig. 2. Aortic arch VC was assessed by quantifying pulse wave velocity (PWV) using non-ECG triggered 1D PC-MRI projection technique. a) the axial reference image, b) the 1D projection image, c) a representative oblique sagittal image, and d) velocity waveforms in the ascending (Aa) and descending (Da) aorta. The imaging plane of PWV was shown in Fig. 1. The path length (ΔD) of the pressure wave from the ascending (Aa) to proximal descending (Da) aorta was estimated by manually drawing a line in the center of the aorta from oblique sagittal image (c) of the aorta. The position of high signal intensity in the projection image (b) corresponds to the location of Aa and Da during systole. The propagation time (Δt) in (d) from the location of Aa to Da was calculated from projection image (b). Aortic PWV was computed as ΔD/Δt.

the perfusion weighted signal of all the time points (TIs) in one measurement was beyond one SD from the mean [$S_{mean}(t) - SD(t)$, $S_{mean}(t) + SD(t)$], the ASL data at all the time points of that measurement was excluded.

After intra-scan outlier rejection, CBV maps were generated (Yan et al., 2012) from the systolic and diastolic dynamic ASL scan, respectively. The 2D rigid in-plane motion estimation was performed between the systolic and diastolic CBV maps using the FSL *flirt* function, by which both rotation matrix and translation matrix were obtained. The 2D motion displacement (MD) was calculated by Eq. (1),

$$MD = |\Delta d_x| + |\Delta d_y| + |\Delta\alpha| \quad (1)$$

where Δd_x, Δd_y, and $\Delta\alpha$ were the 2D rigid body motion parameters representing translation in x and y directions and in-plane rotation respectively. The rotational displacement $\Delta\alpha$ was converted from degrees to millimeters by calculating the displacement on a spherical surface with the radius of 50 mm (Power et al., 2012). If MD > 1 mm, the VC data were excluded from further analyses.

VC quantification

Arterial CBV (aCBV) maps were calculated from the data acquired by dynamic ASL bSSFP sequence by Eq. (2) (Yan et al., 2012) following image outlier rejection.

$$aCBV = \frac{\int C(t)e^{t/T_{1,blood}}dt}{\int C_a(t)e^{t/T_{1,blood}}dt} \quad (2)$$

where $C_a(t)$ and $C(t)$ represent the concentration of labeled spins in the artery and each pixel respectively, and T_{1blood} is the T_1 relaxation time of arterial blood (1.65 s at 3 T) (Lu et al., 2004). The arterial input function $C_a(t)$ was derived from one or two pixels within large arteries that showed the earliest peak. Two ROIs were defined i.e., large arteries with CBV > 5% (the size of ROI: 10.12 ± 4.20 cm^3), and small arteries and arterioles with CBV of 1.5–5% (the size of ROI: 33.07 ± 14.23 cm^3) in the entire slice. The CBV threshold for large and small arteries was based on a mean total CBV of ~5% and mean arterial CBV of ~1.5% in the literature (Ge et al., 2006). Dynamic time courses of the labeled

blood signal were derived from the two ROIs of each subject, which were normalized by the corresponding peak value of the diastolic curve. To calculate the absolute CBV instead of fractional CBV (of the brain volume), the brain volume of each subject was measured from the MPRAGE images (Jain et al., 2012). The absolute arterial CBV values were obtained in large arteries and small arteries/arterioles. VC was calculated by Eq. (3), where the difference between $BP_{systole}$ and $BP_{diastole}$ was directly derived from pulse pressure (PP) using a MR compatible cuff sphygmomanometer.

$$VC = \frac{CBV_{systole} - CBV_{diastole}}{BP_{systole} - BP_{diastole}} \quad (3)$$

CBF and PWV quantification

Perfusion images were generated from 3D GRASE pCASL data by pairwise subtraction between the control and tag pairs, after head motion correction. Quantitative CBF maps were calculated based on a standard one compartment model (Wang et al., 2005), assuming a labeling efficiency of 0.77 by taking into account the loss of efficiency by two background suppression pulses (Kilroy et al., 2014), and blood T1 of 1650 ms at 3 T (Lu et al., 2004). The MPRAGE images were segmented into gray matter, white matter and cerebrospinal fluid (CSF) using SPM8. Mean CBF was extracted from a gray matter mask thresholded for probabilities above 90% for each subject.

Aortic PWV was estimated from the 1D projection-based PC MRI data. The complex difference signal intensity from two successive projections with and without velocity encoding along slice direction (i.e. along the axis of the body) has approximately a linear relationship with the blood flow velocity (Langham et al., 2011a). Thus the time-resolved complex difference signal intensity curve can approximate the velocity–time curve at the foot of the systolic upstroke. The path length (ΔD) of the pressure wave from the ascending to proximal descending aorta was measured manually by drawing a line in the center of the aorta from the oblique sagittal image of the aorta (Fig. 2). The average temporal separation (Δt) was estimated at the lower-third of the upstroke of the signal curve between ascending and descending aorta; and the PWV was computed as ΔD/Δt.

Statistical analyses

Statistical analyses were performed using SPSS 19.0 software package (SPSS Inc., Chicago, IL). VC data were compared between the young and elderly groups using two sample t-test to investigate the aging effect on VC. Two-tailed p value of 0.05 or less was considered to indicate a significant difference. Pearson correlation was performed between VC and CBF or PWV measurements across subjects. The correlation analysis was further performed with age included as a covariate.

Results

VC in different cerebrovascular components

Figs. 3a, b show the CBV maps from a representative young subject at systole and diastole, respectively. The map of CBV difference between systole and diastole is shown in Fig. 3c. It can be clearly seen that the CBV change primarily occurs in the large arteries (M2/M3 in MCA and, P2/P3 in PCA), and to a lesser extent in small arteries and arterioles. Fig. 4 shows the mean normalized time courses in each vascular component at systole (red) and diastole (blue) using the dynamic ASL bSSFP sequence (Figs. 4a,b) and Look-Locker EPI ASL sequence (Fig. 4c). Elevated labeled blood signals can be observed for the peak systolic time courses in large arteries as well as in small arteries and arterioles. However, there was no perceivable difference between dynamic capillary/tissue perfusion signals between systolic and diastolic phases. The mean VC from the young subjects was estimated to be 0.21 ± 0.01 mL/mm Hg and 0.09 ± 0.003 mL/mm Hg in large arteries and small arteries/arterioles, respectively.

Aging effects on intracranial VC

Figs. 3d, e and f show the CBV maps at systole and diastole and the change of CBV (ΔCBV) from a representative elderly subject,

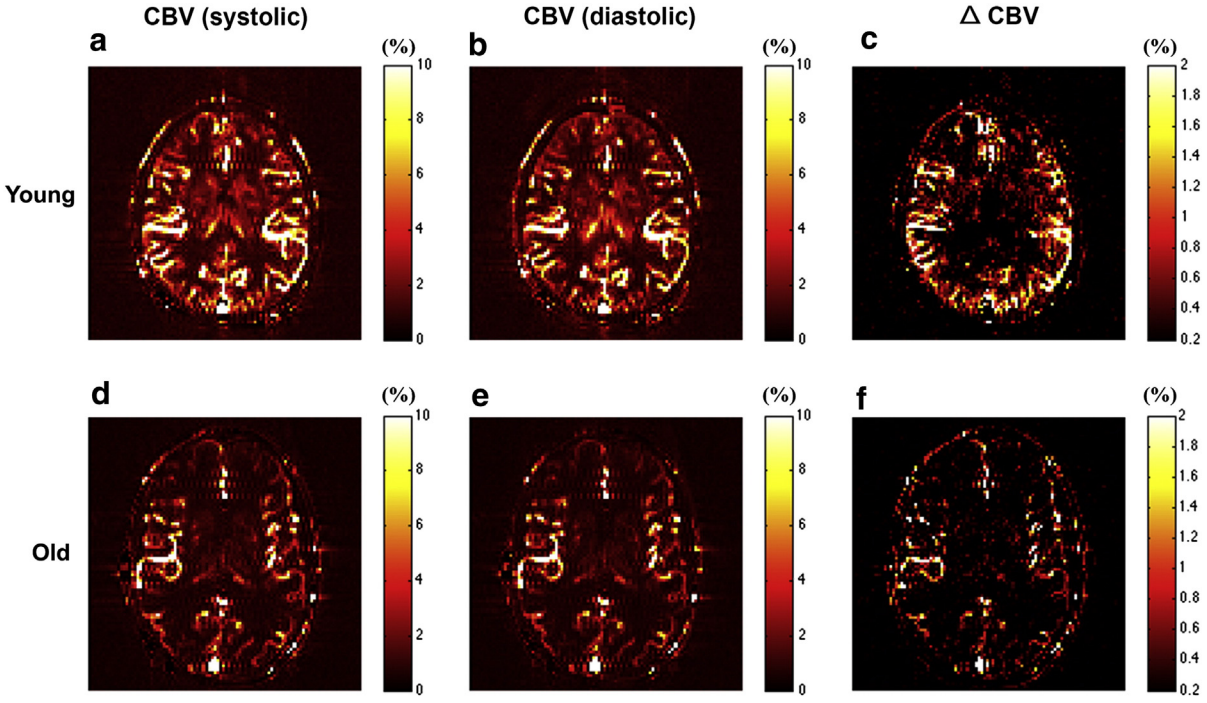

Fig. 3. Representative maps of CBV at systole and early diastole, as well as the corresponding CBV change (ΔCBV) between systole and diastole from a young (21 years, male) (a, b and c) and elderly (59 years, male)(d, e and f) subject, respectively.

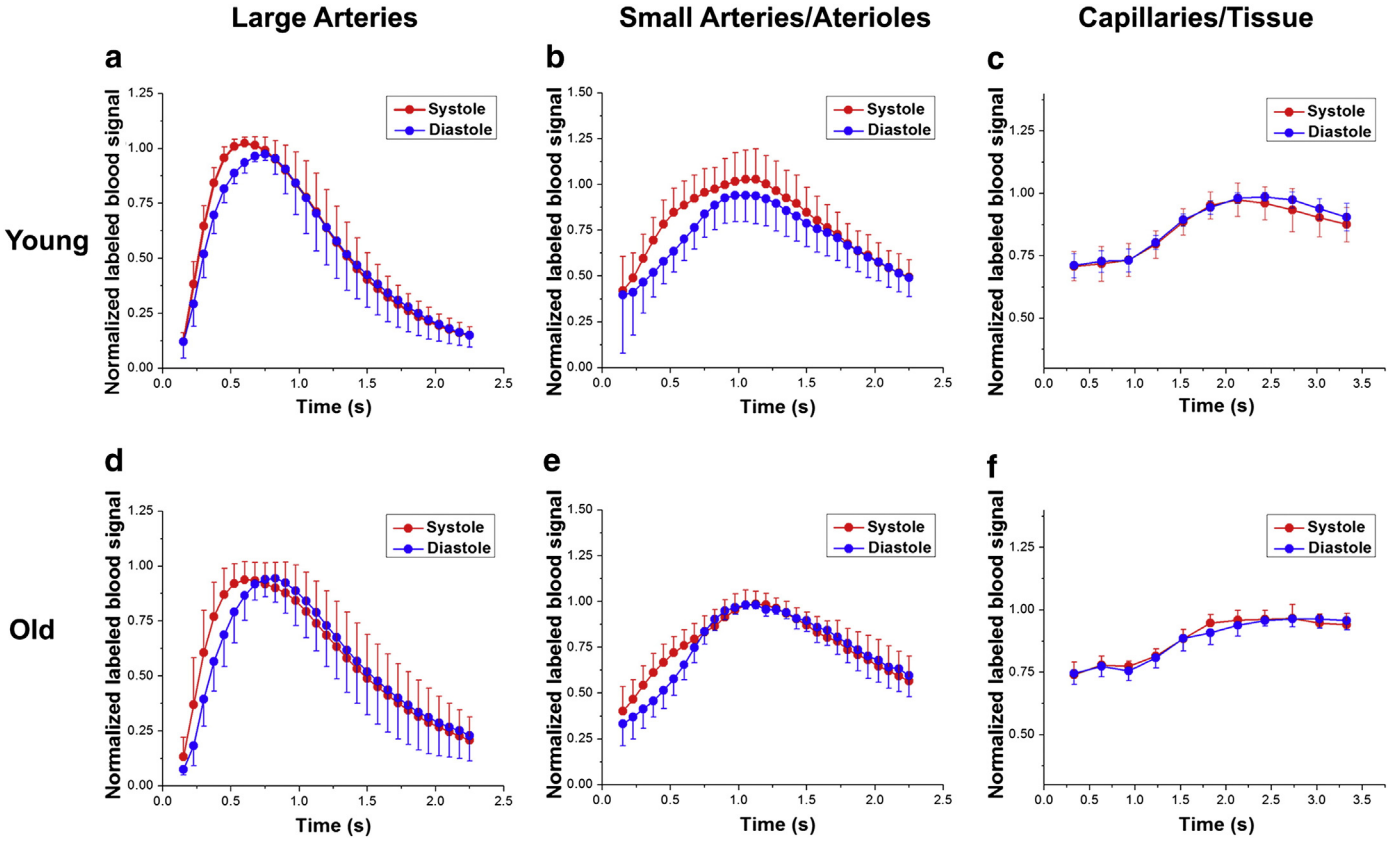

Fig. 4. Mean normalized time courses of multi-phase bSSFP and LL-EPI ASL signals from young(a, b and c) and elderly(d, e and f) subjects with spin tagging applied at the peak systolic (red) and early diastolic (blue) phases in large arteries (a and d), small arteries/arterioles (b and e), and capillary/tissue (c and f) respectively. Error bars indicate standard deviation (SD).

respectively. A reduced ΔCBV can be seen, compared to the young subjects, especially in small arteries/arterioles. The mean normalized time course of dynamic ASL signals at systole and diastole were shown in different vascular components from the elderly subjects in Figs. 4 d, e and f. Compared to the young subjects, the difference between systolic and diastolic time courses is visibly reduced. Particularly, instead of elevated signal at systole, a temporal shift between systolic and diastolic curves was observed in the large arteries from the elderly subjects. The quantitative ΔCBV, PP and VC from both the young (black color bars) and elderly (red color bars) subjects are shown in Fig. 5. Consistent with the visual appearance of the ΔCBV map, greater ΔCBV was observed in large arteries from both the young and elderly subjects. A decrease of ΔCBV in both large arteries ($p = 0.0013$) and small arteries/arterioles ($p = 0.0072$) as well as an increase of pulse pressure ($p = 0.0022$) between systolic and diastolic phases were observed in elderly subjects, resulting in a markedly reduced VC in elderly subjects (0.061 ± 0.004 mL/mm Hg and 0.025 ± 0.003 mL/mm Hg in large arteries and small arteries/arterioles, respectively).

Relationship between intracranial VC and cerebral perfusion

In the present and following PWV analysis, we focused on ΔCBV and VC measures in the arterial ROI (CBV > 5%) given the higher SNR and more reliable measurements. Fig. 6a shows the scatter plot of VC as a function of age across the eighteen subjects. A reduction of VC with age ($r = -0.52$, $p = 0.026$) was observed, which is consistent with the finding shown in Fig. 5. Fig. 6b shows the scatter plot between global CBF measured by 3D GRASE pCASL and age across subjects, which indicates a significant trend of decreasing gray matter (GM) CBF with aging ($r = -0.49$, $p = 0.041$). Fig. 6c shows the scatter plot between VC and CBF across subjects. A highly significant positive correlation between VC and CBF was observed ($r = 0.71$, $p = 0.01$), suggesting that subjects

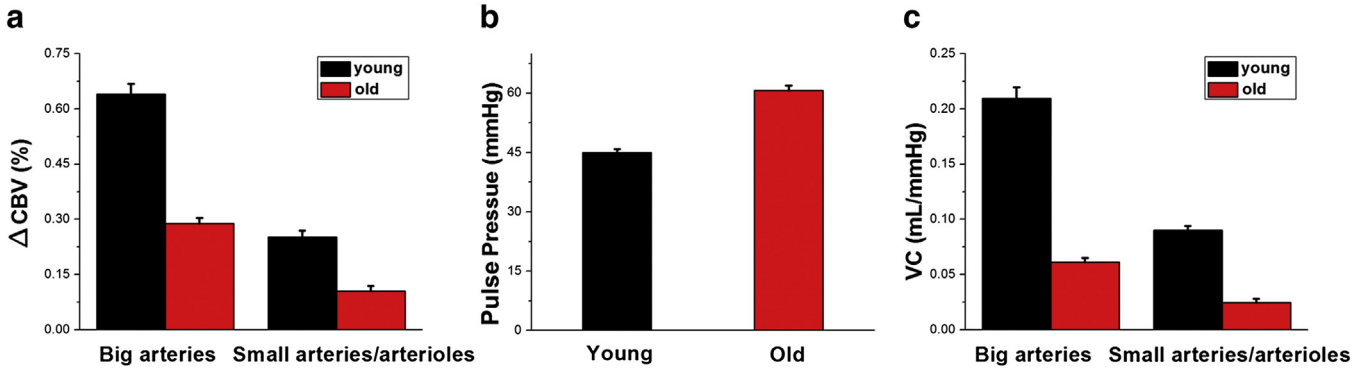

Fig. 5. Comparison of CBV changes (a), pulse pressure (b), and vascular compliance (c) between young and elderly subjects. Error bars indicate the standard error (SE).

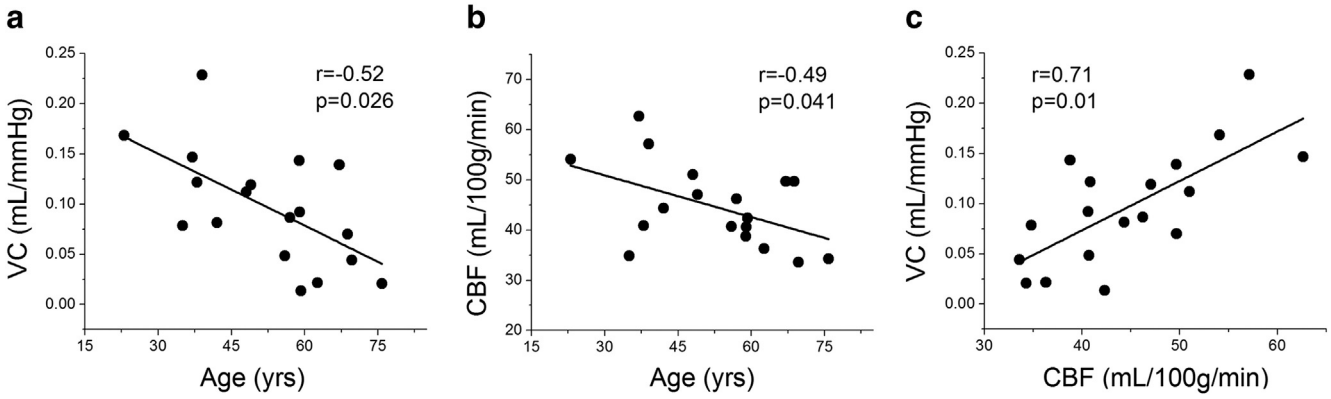

Fig. 6. a) Scatter plots between VC and age, b) CBF and age, c) CBF and VC across subjects. R and p values were shown in each sub-figure.

with reduced intracranial VC also had lower perfusion. This association between intracranial VC and perfusion persisted when age was included as a covariate in regression analysis ($r = 0.60$, $p = 0.012$).

Relationship between intracranial VC and aortic PWV

Aortic PWV was successfully estimated using non-ECG triggered 1D projection-based PC MRI. Fig. 7 shows the scatter plot of intracranial VC and aortic PWV. Intracranial VC exhibited a significant negative correlation with aortic PWV ($r = -0.74$, $p = 0.013$). Such correlation between intracranial and aortic VC persisted when age was included as a covariate in regression analysis ($r = -0.73$, $p = 0.024$).

Discussion

In the present study, a novel non-invasive method was introduced for assessing intracranial VC using ECG-gated dynamic ASL with multiphase cine bSSFP readout. We demonstrated arterial CBV expansion to comply with arterial pressure differences between the peak systolic vs. early diastolic phases. Using this technique, we confirmed that, in the brain, large arteries are more compliant than small arteries and arterioles. Additionally, there is no difference of dynamic perfusion signals observed in capillaries between systole and diastole. This buffering action of arteries plays an important role in the protection of the whole cerebrovascular system by converting the pulsatile stroke volume to continuous flow into the capillaries. As a result, capillary and tissue perfusion is stable across cardiac cycles as a potential mechanism to protect capillary endothelium and the blood–brain barrier.

Aortic stiffening, or decreased central VC, has long been observed in aging due to the loss of elastin content and replacement by collagen (Lee and Oh, 2010; Mohiaddin et al., 1993; Van Bortel and Spek, 1998). Using the proposed method, a decreased intracranial VC with aging was directly observed in intracranial arteries. When vascular compliance is diminished, the buffering capability of the vasculature decreases. Instead of continuous flow, pulsatile flow might extend into the small arteries, which over time might damage downstream vasculature and impair perfusion or cerebral vasoreactivity (CVR). In the present study, a strong positive correlation between intracranial VC and cerebral blood perfusion was observed, independent of age effects. It is likely that loss of VC and CVR precedes decline in perfusion. Although the relationship between intracranial VC and cerebral perfusion requires further systematic evaluation in larger populations, the observed association between intracranial VC and perfusion supports the validity of the proposed VC technique.

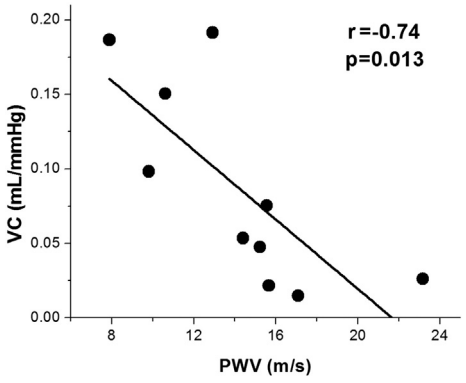

Fig. 7. Scatter plot between measured VC and PWV values across subjects. A significant negative correlation was observed between VC and PWV data.

As a non-invasive approach, PWV offers a simple and reliable method to indirectly estimate central and peripheral VC, which can be assessed using ultrasound and MRI (Langham et al., 2011a; Sutton-Tyrrell et al., 2005; Tanaka et al., 2009). However, the main limitation of PWV is that only large central and peripheral arterial segments can be assessed. It is thought that aortic stiffening leads to cerebral arterial stiffening (Hughes et al., 2013; Nation et al., 2012; Qiu et al., 2003). To investigate the relationship between intracranial and central arterial stiffening, we compared intracranial VC with aortic PWV. A negative correlation ($r = -0.74$, $p = 0.013$) was obtained in this study. PWV is an index of arterial stiffness, which is inversely related to VC. Therefore a positive correlation between intracranial and aortic VC was expected, suggesting a link between central (aortic) and cerebral (intracranial) arterial stiffening (Mitchell, 2008). However, intracranial arterial stiffening may be caused by different physiological events such as accumulation of amyloid along vessel walls compared to those underlying aortic stiffening (e.g., loss of elastin content and replacement by collagen). The relationship between intracranial VC and PWV awaits further investigation in larger populations.

Arterial stiffening has been regarded as a significant risk marker for cardio- and cerebrovascular disease as well as Alzheimer's disease (Blacher et al., 1999; McVeigh et al., 1991; Meaume et al., 2001b; Scuteri et al., 2007; Sutton-Tyrrell et al., 2005). Mounting evidence suggests that intracranial vascular pathology (e.g. breakdown of blood–brain barrier) precedes and may cause parenchymal and intravascular AD pathology (i.e. amyloid plaques and neurofibrillary tangles, and amyloid angiopathy) (Hughes et al., 2013; Zlokovic, 2011). Recently, a vascular hypothesis of AD has emerged, which posits that cerebrovascular dysfunctions, such as arterial stiffening, loss of autoregulation, oligemia, and breakdown of blood–brain barrier, likely precede and may even cause vascular and parenchymal amyloid deposition (Zlokovic, 2011). In the cascade of vascular changes associated with AD, stiffening of intracranial arteries and arterioles might be one of the earliest. Cerebral arterial stiffening results in amyloid accumulation in the vessel walls, because of decrease in interstitial fluid flow that removes amyloid. Subsequently parenchymal amyloid plaque accumulation follows progressive disruption of beta-amyloid clearance in the blood–brain barrier.

Therefore, intracranial VC is likely to be an important marker for vascular pathology in the earliest stages of AD, understanding of which may be critical for the development of therapy. A recent study by Hughes et al. (2014) showed a strong positive correlation between extracranial arterial stiffening (PWV in aorta, brachial arteries, and femoral arteries) and cerebral amyloid deposition and progression, independent of hypertension. Our finding of significant associations between intracranial VC, cerebral perfusion and aortic PWV is an extension of the association between extracranial (i.e. aorta) arterial stiffening and cerebral hypoperfusion in vascular risks and AD (Hughes et al., 2013, 2014), to intracranial arteries. Therefore, intracranial VC may be used as an early imaging marker of AD.

Dynamic pressure–flow relationship of cerebral circulation can be used to assess dynamic cerebral autoregulation using transcranial Doppler (TCD) combined with measurement of arterial blood pressure, which is affected by alterations in steady-state cerebrovascular resistance and vascular compliance (Aaslid et al., 1989; Zhang et al., 1998). A Windkessel model can be used to describe the dynamic pressure–flow relationship, from which the vascular compliance can be derived (Olufsen et al., 2002; Zhang et al., 2009). For instance, Zhang et al. (2009) used a three-element Windkessel model to derive vascular compliance. Based on their simulation, cerebral vascular compliance was given within the range of 0–0.5 mL/mm Hg. In addition, cerebral compliance was invasively assessed in past studies (Portella et al., 2002; Purins et al., 2011; Yau et al., 2000). The intracranial vascular compliance is recognized as one of the most important components contributing to cerebral compliance. Purins et al. (2011) reported that the intracranial compliance decreased from 0.137 ± 0.069 mL/mm Hg to 0.007 ± 0.001 mL/mm Hg after balloon infusion in the pig. Yau et al. (2000) measured the intracranial compliance within a range of 0.05 to 0.3 mL/mm Hg in sheep. Portella et al. (2002) measured the cerebral compliance in severe traumatic brain injured patients, which was 0.51 ± 0.3 mL/mm Hg and 0.64 ± 0.3 mL/mm Hg when cerebral perfusion pressure was above and below 60 mm Hg, respectively. In the present study, the measured intracranial VC values using dynamic ASL approach was 0.21 ± 0.01 mL/mm Hg and 0.061 ± 0.004 mL/mm Hg in large arteries (M2 and M3 in MCA) and 0.09 ± 0.003 mL/mm Hg and 0.025 ± 0.003 mL/mm Hg in small arteries/arterioles from the healthy young and elderly subjects, respectively, which are in a reasonable range compared to those reported in the literature.

There are several limitations of this work. According to the definition of VC, VC is calculated by CBV change due to a given change of blood pressure at the same arterial segment. Until now, there is no valid method to noninvasively measure the intracranial arterial blood pressure. Normally, the pulse pressure in carotid arteries is approximately 11–14 mm Hg lower than brachial pulse pressure, both in normotensive and hypertensive subjects. This difference contributes to the protection of the heart from an increased after-load (Safar and O'Rourke, 2006). Therefore, there is a systematic underestimation of VC in our method. On the other hand, the pulse pressure may decrease from large to small cerebral arteries (Safar and Lacolley, 2007) which may contribute to the observed decline in VC from large arteries to small arteries and arterioles. Future work is required to assess the difference in pulse pressure between intracranial and peripheral arteries as well as between different cerebrovascular components. Secondly, intracranial VC was only measured from a single 2D slice. To improve the accuracy and reliability of VC measurement, a single slice with multiple repetitions was acquired which took 3 min using the existing technique, leading to a relative long scan time to cover multiple slices. In future work, three-dimensional acquisitions can be adapted to improve the imaging efficiency for volumetric measurement of VC, which allow effective motion correction. Third, VC of smaller arteries is not simply a function of elastin and collagen content. It has a reactive component, which can be influenced by vasoactive substances (e.g. medication and caffeine), medical history (e.g. hypertension and diabetes), and hormones (e.g. angiotensin). A larger sample size will be needed to determine their effects as well as comparison between passive VC and active CVR. This technique might help discover other risk factors for intracranial arterial stiffening.

Conclusion

A novel non-invasive method was introduced to assess intracranial vascular compliance using a dynamic ASL approach. Intracranial VC is most pronounced in large arteries, with observed decrease in smaller arteries/arterioles. Aging was accompanied by a reduction of VC. The decrease of intracranial VC was also associated with reduced perfusion as well as decreasing aortic VC.

Acknowledgment

The authors are grateful to Dr. Cheng Li for assistance with PWV processing. This work was supported by NIH grants R01-MH080892; R01-NS081077; R01-EB014922; P50-AG016570; K25 HL111422; California Department of Public Health grant CDPH 13-12008.

References

Aaslid, R., Lindegaard, K.F., Sorteberg, W., Nornes, H., 1989. Cerebral autoregulation dynamics in humans. Stroke 20, 45–52.
Blacher, J., Asmar, R., Djane, S., London, G.M., Safar, M.E., 1999. Aortic pulse wave velocity as a marker of cardiovascular risk in hypertensive patients. Hypertension 33, 1111–1117.
Boese, J.M., Bock, M., Schoenberg, S.O., Schad, L.R., 2000. Estimation of aortic compliance using magnetic resonance pulse wave velocity measurement. Phys. Med. Biol. 45, 1703–1713.
Chen, Y., Wang, D.J., Detre, J.A., 2012. Comparison of arterial transit times estimated using arterial spin labeling. MAGMA 25, 135–144.
Detre, J.A., Wang, J., Wang, Z., Rao, H., 2009. Arterial spin-labeled perfusion MRI in basic and clinical neuroscience. Curr. Opin. Neurol. 22, 348–355.
Ge, H., Xu, J., Zhou, X., 2006. Decision support for tendon tissue engineering. J. Med. Eng. Technol. 30, 69–72.
Golay, X., Hendrikse, J., Lim, T.C., 2004. Perfusion imaging using arterial spin labeling. Top. Magn. Reson. Imaging 15, 10–27.
Hughes, T.M., Kuller, L.H., Barinas-Mitchell, E.J., Mackey, R.H., McDade, E.M., Klunk, W.E., Aizenstein, H.J., Cohen, A.D., Snitz, B.E., Mathis, C.A., Dekosky, S.T., Lopez, O.L., 2013. Pulse wave velocity is associated with beta-amyloid deposition in the brains of very elderly adults. Neurology 81, 1711–1718.
Hughes, T.M., Kuller, L.H., Barinas-Mitchell, E.J., McDade, E.M., Klunk, W.E., Cohen, A.D., Mathis, C.A., Dekosky, S.T., Price, J.C., Lopez, O.L., 2014. Arterial stiffness and beta-amyloid progression in nondemented elderly adults. JAMA Neurol. 71, 562–568.
Jain, V., Duda, J., Avants, B., Giannetta, M., Xie, S.X., Roberts, T., Detre, J.A., Hurt, H., Wehrli, F.W., Wang, D.J., 2012. Longitudinal reproducibility and accuracy of pseudo-continuous arterial spin-labeled perfusion MR imaging in typically developing children. Radiology 263, 527–536.
Kelly, B.A., Chowienczyk, P., 2002. Vascular compliance. In: Hunt, B.J., Poston, L., Schachter, M., Halliday, A. (Eds.), An Introduction to Vascular Biology: From Basic Science to Clinical Practice. Cambridge University, UK, pp. 33–48.
Kilroy, E., Apostolova, L., Liu, C., Yan, L., Ringman, J., Wang, D.J., 2014. Reliability of two-dimensional and three-dimensional pseudo-continuous arterial spin labeling perfusion MRI in elderly populations: comparison with 15O-water positron emission tomography. J. Magn. Reson. Imaging 39, 931–939.
Laffon, E., Marthan, R., Montaudon, M., Latrabe, V., Laurent, F., Ducassou, D., 2005. Feasibility of aortic pulse pressure and pressure wave velocity MRI measurement in young adults. J. Magn. Reson. Imaging 21, 53–58.
Langham, M.C., Li, C., Magland, J.F., Wehrli, F.W., 2011a. Nontriggered MRI quantification of aortic pulse-wave velocity. Magn. Reson. Med. 65, 750–755.
Langham, M.C., Li, C., Wehrli, F.W., 2011b. Non-triggered quantification of central and peripheral pulse-wave velocity. J. Cardiovasc. Magn. Reson. 13, 81.
Laurent, S., Boutouyrie, P., Asmar, R., Gautier, I., Laloux, B., Guize, L., Ducimetiere, P., Benetos, A., 2001. Aortic stiffness is an independent predictor of all-cause and cardiovascular mortality in hypertensive patients. Hypertension 37, 1236–1241.
Laurent, S., Katsahian, S., Fassot, C., Tropeano, A.I., Gautier, I., Laloux, B., Boutouyrie, P., 2003. Aortic stiffness is an independent predictor of fatal stroke in essential hypertension. Stroke 34, 1203–1206.
Lee, H.Y., Oh, B.H., 2010. Aging and arterial stiffness. Circ. J. 74, 2257–2262.
Lu, H., Clingman, C., Golay, X., van Zijl, P.C., 2004. Determining the longitudinal relaxation time (T1) of blood at 3.0 Tesla. Magn. Reson. Med. 52, 679–682.
Mackenzie, I.S., Wilkinson, I.B., Cockcroft, J.R., 2002. Assessment of arterial stiffness in clinical practice. QJM 95, 67–74.
McVeigh, G.E., Burns, D.E., Finkelstein, S.M., McDonald, K.M., Mock, J.E., Feske, W., Carlyle, P.F., Flack, J., Grimm, R., Cohn, J.N., 1991. Reduced vascular compliance as a marker for essential hypertension. Am. J. Hypertens. 4, 245–251.
Meaume, S., Benetos, A., Henry, O.F., Rudnichi, A., Safar, M.E., 2001a. Aortic pulse wave velocity predicts cardiovascular mortality in subjects >70 years of age. Arterioscler. Thromb. Vasc. Biol. 21, 2046–2050.

Meaume, S., Rudnichi, A., Lynch, A., Bussy, C., Sebban, C., Benetos, A., Safar, M.E., 2001b. Aortic pulse wave velocity as a marker of cardiovascular disease in subjects over 70 years old. J. Hypertens. 19, 871–877.
Mitchell, G.F., 2008. Effects of central arterial aging on the structure and function of the peripheral vasculature: implications for end-organ damage. J. Appl. Physiol. 105, 1652–1660.
Mohiaddin, R.H., 1992. Magnetic resonance imaging of peripheral vascular disease. The state of the artery. Echocardiography 9, 553–577.
Mohiaddin, R.H., Firmin, D.N., Longmore, D.B., 1993. Age-related changes of human aortic flow wave velocity measured noninvasively by magnetic resonance imaging. J. Appl. Physiol. 74, 492–497.
Nation, D.A., Delano-Wood, L., Bangen, K.J., Wierenga, C.E., Jak, A.J., Hansen, L.A., Galasko, D.R., Salmon, D.P., Bondi, M.W., 2012. Antemortem pulse pressure elevation predicts cerebrovascular disease in autopsy-confirmed Alzheimer's disease. J. Alzheimers Dis. 30, 595–603.
Nelson, M.R., Stepanek, J., Cevette, M., Covalciuc, M., Hurst, R.T., Tajik, A.J., 2010. Noninvasive measurement of central vascular pressures with arterial tonometry: clinical revival of the pulse pressure waveform? Mayo Clin. Proc. 85, 460–472.
Olufsen, M.S., Nadim, A., Lipsitz, L.A., 2002. Dynamics of cerebral blood flow regulation explained using a lumped parameter model. Am. J. Physiol. Regul. Integr. Comp. Physiol. 282, R611–R622.
Ostergaard, L., Weisskoff, R.M., Chesler, D.A., Gyldensted, C., Rosen, B.R., 1996. High resolution measurement of cerebral blood flow using intravascular tracer bolus passages. Part I: Mathematical approach and statistical analysis. Magn. Reson. Med. 36, 715–725.
Portella, G., Cormio, M., Citerio, G., 2002. Continuous cerebral compliance monitoring in severe head injury: its relationship with intracranial pressure and cerebral perfusion pressure. Acta Neurochir. Suppl. 81, 173–175.
Power, J.D., Barnes, K.A., Snyder, A.Z., Schlaggar, B.L., Petersen, S.E., 2012. Spurious but systematic correlations in functional connectivity MRI networks arise from subject motion. NeuroImage 59, 2142–2154.
Purins, K., Sedigh, A., Molnar, C., Jansson, L., Korsgren, O., Lorant, T., Tufveson, G., Wennberg, L., Wiklund, L., Lewen, A., Enblad, P., 2011. Standardized experimental brain death model for studies of intracranial dynamics, organ preservation, and organ transplantation in the pig. Crit. Care Med. 39, 512–517.
Qiu, C., Winblad, B., Viitanen, M., Fratiglioni, L., 2003. Pulse pressure and risk of Alzheimer disease in persons aged 75 years and older: a community-based, longitudinal study. Stroke 34, 594–599.
Romney, J.S., Lewanczuk, R.Z., 2001. Vascular compliance is reduced in the early stages of type 1 diabetes. Diabetes Care 24, 2102–2106.
Safar, M.E., Lacolley, P., 2007. Disturbance of macro- and microcirculation: relations with pulse pressure and cardiac organ damage. Am. J. Physiol. Heart Circ. Physiol. 293, H1–H7.
Safar, M.E., O'Rourke, M.F., 2006. Arterial Stiffness in Hypertension: Handbook of Hypertension. Elsevier.
Scuteri, A., Tesauro, M., Appolloni, S., Preziosi, F., Brancati, A.M., Volpe, M., 2007. Arterial stiffness as an independent predictor of longitudinal changes in cognitive function in the older individual. J. Hypertens. 25, 1035–1040.
Sutton-Tyrrell, K., Najjar, S.S., Boudreau, R.M., Venkitachalam, L., Kupelian, V., Simonsick, E.M., Havlik, R., Lakatta, E.G., Spurgeon, H., Kritchevsky, S., Pahor, M., Bauer, D., Newman, A., 2005. Elevated aortic pulse wave velocity, a marker of arterial stiffness, predicts cardiovascular events in well-functioning older adults. Circulation 111, 3384–3390.
Tanaka, H., Munakata, M., Kawano, Y., Ohishi, M., Shoji, T., Sugawara, J., Tomiyama, H., Yamashina, A., Yasuda, H., Sawayama, T., Ozawa, T., 2009. Comparison between carotid-femoral and brachial-ankle pulse wave velocity as measures of arterial stiffness. J. Hypertens. 27, 2022–2027.
Tarumi, T., Shah, F., Tanaka, H., Haley, A.P., 2011. Association between central elastic artery stiffness and cerebral perfusion in deep subcortical gray and white matter. Am. J. Hypertens. 24, 1108–1113.
Van Bortel, L.M., Spek, J.J., 1998. Influence of aging on arterial compliance. J. Hum. Hypertens. 12, 583–586.
van Popele, N.M., Grobbee, D.E., Bots, M.L., Asmar, R., Topouchian, J., Reneman, R.S., Hoeks, A.P., van der Kuip, D.A., Hofman, A., Witteman, J.C., 2001. Association between arterial stiffness and atherosclerosis: the Rotterdam Study. Stroke 32, 454–460.
Wang, J., Zhang, Y., Wolf, R.L., Roc, A.C., Alsop, D.C., Detre, J.A., 2005. Amplitude-modulated continuous arterial spin-labeling 3.0-T perfusion MR imaging with a single coil: feasibility study. Radiology 235, 218–228.
Wentland, A.L., Grist, T.M., Wieben, O., 2014. Review of MRI-based measurements of pulse wave velocity: a biomarker of arterial stiffness. Cardiovasc. Diagn. Ther. 4, 193–206.
Wilkinson, I.B., Fuchs, S.A., Jansen, I.M., Spratt, J.C., Murray, G.D., Cockcroft, J.R., Webb, D.J., 1998. Reproducibility of pulse wave velocity and augmentation index measured by pulse wave analysis. J. Hypertens. 16, 2079–2084.
Wu, W.C., Jain, V., Li, C., Giannetta, M., Hurt, H., Wehrli, F.W., Wang, D.J., 2010. In vivo venous blood T1 measurement using inversion recovery true-FISP in children and adults. Magn. Reson. Med. 64, 1140–1147.
Yan, L., Li, C., Kilroy, E., Wehrli, F.W., Wang, D.J., 2012. Quantification of arterial cerebral blood volume using multiphase-balanced SSFP-based ASL. Magn. Reson. Med. 68, 130–139.
Yau, Y.H., Piper, I.R., Clutton, R.E., Whittle, I.R., 2000. Experimental evaluation of the Spiegelberg intracranial pressure and intracranial compliance monitor. Technical note. J. Neurosurg. 93, 1072–1077.
Zhang, R., Zuckerman, J.H., Giller, C.A., Levine, B.D., 1998. Transfer function analysis of dynamic cerebral autoregulation in humans. Am. J. Physiol. 274, H233–H241.
Zhang, R., Behbehani, K., Levine, B.D., 2009. Dynamic pressure–flow relationship of the cerebral circulation during acute increase in arterial pressure. J. Physiol. 587, 2567–2577.
Zlokovic, B.V., 2011. Neurovascular pathways to neurodegeneration in Alzheimer's disease and other disorders. Nat. Rev. Neurosci. 12, 723–738.